Correlation of the superconducting critical temperature with spin and orbital excitations in $(Ca_xLa_{1-x})(Ba_{1.75-x}La_{0.25+x})Cu_3O_y$ as measured by resonant inelastic x-ray scattering

David Shai Ellis,[1] Yao-Bo Huang,[2,3] Paul Olalde-Velasco,[2] Marcus Dantz,[2] Jonathan Pelliciari,[2] Gil Drachuck,[1] Rinat Ofer,[1] Galina Bazalitsky,[1] Jorge Berger,[4] Thorsten Schmitt,[2] and Amit Keren[1,*]

[1]*Physics Department, Technion-Israel Institute of Technology, Haifa 32000, Israel*

[2]*Swiss Light Source, Paul Scherrer Institut, CH-5232 Villigen PSI, Switzerland*

[3]*Beijing National Laboratory for Condensed Matter Physics, and Institute of Physics, Chinese Academy of Sciences, Beijing 100190, China*

[4]*Department of Physics and Optical Engineering, ORT-Braude College, P.O. Box 78, 21982, Karmiel, Israel*

(Received 31 December 2014; revised manuscript received 11 June 2015; published 10 September 2015)

Electronic spin and orbital (dd) excitation spectra of $(Ca_xLa_{1-x})(Ba_{1.75-x}La_{0.25+x})Cu_3O_y$ samples are measured by resonant inelastic x-ray scattering (RIXS). In this compound, T_c of samples with identical hole dopings is strongly affected by the Ca/Ba substitution x due to subtle variations in the lattice constants, while crystal symmetry and disorder as measured by linewidths are x independent. We examine two extreme values of x and two extreme values of hole-doping content y corresponding to antiferromagnetic and superconducting states. The x dependence of the spin-mode energies is approximately the same for both the antiferromagnetic and superconducting samples. This clearly demonstrates that RIXS is sensitive to the superexchange J even in doped samples. A positive correlation between J and the maximum of T_c at optimal doping ($T_c^{\max}$) is observed. We also measured the x dependence of the $d_{xy} \rightarrow d_{x^2-y^2}$ and $d_{xz/yz} \rightarrow d_{x^2-y^2}$ orbital splittings. We infer that the effect of the unresolved $d_{3z^2-r^2} \rightarrow d_{x^2\rightarrow y^2}$ excitation on $T_c^{\max}$ is much smaller than the effect of J. There appears to be dispersion in the $d_{xy} \rightarrow d_{x^2-y^2}$ peak of up to 0.05 eV. Our fitting furthermore indicates an asymmetric dispersion for the $d_{xz/yz} \rightarrow d_{x^2-y^2}$ excitation. A peak at ~0.8 eV is also observed and attributed to a dd excitation in the chain layer.

DOI: 10.1103/PhysRevB.92.104507 PACS number(s): 74.62.Bf, 74.72.Gh, 75.30.Ds, 78.70.Ck

I. INTRODUCTION

Theories built around coupling of the electron spins **S** have become the prominent models for high-T_c superconductivity [1]. A key parameter in these theories is the magnetic superexchange energy J, which is predicted to limit [2] or set [3,4] the critical temperature for superconductivity. One method of testing this has been to compare T_c against J for a variety of cuprates [5–8]. The study of Munoz *et al.* [5] resulted in $\Delta T_c^{\max}/\Delta J \sim 3$ K/meV. However, if the compounds vary in structures and nuances, other factors besides J are likely to influence the J-T_c plot, which are a likely source of scatter in the plot of Ref. [5]. Another approach has been to measure the effect of pressure on a single compound. For the case of $YBa_2Cu_3O_y$ (YBCO), T_c has been found to initially increase under hydrostatic pressure [9–12]. Under pressure, J also increases [7], yielding $\Delta T_c^{\max}/\Delta J \sim 1.5$ K/meV. While similar orders of magnitude are encouraging, it shows that the fluctuations in the slope could be large depending on materials or conditions. In fact, Mallet *et al.* [7] observed a negative J-T_c slope in a series of $RA_2Cu_3O_y$ compounds with $A = (Ba,Sr)$ $R = (La,...,Lu,Y)$, casting doubt on the spin-mediated scenarios.

Another key parameter thought to strongly affect the cuprates is the $d_{3z^2-r^2} \rightarrow d_{x^2-y^2}$ orbital splitting [13–18]. This splitting increases with increasing apical oxygen distance d_A from the copper-oxygen plane. When the splitting grows, it increases the in-plane character of the holes, creating a condition favorable for superconductivity by stabilizing the Zhang-Rice singlet [13] or rounding the Fermi surface [15]. A higher d_A also reduces screening from polarizable charge reservoir layers [19]. All three options are expected to lead to higher T_c.

The multitude of different control parameters for $T_c^{\max}$ emphasizes the importance of measuring their effects in isolation. Here we measure both J and orbital splitting in $(Ca_xLa_{1-x})(Ba_{1.75-x}La_{0.25+x})Cu_3O_y$ (CLBLCO), using resonant inelastic x-ray scattering (RIXS). CLBLCO, whose phase diagram is shown in Fig. 1, is a compound which allows the tuning of structural parameters independently of the hole doping. Its structure is almost identical to YBCO [20], but it is tetragonal and its chain layers are not ordered. The oxygen content y controls the number of doped holes, only slightly affecting the lattice parameter. In complementary fashion, Ca/Ba content x changes only structural parameters such as bond length a, buckling angles θ, and apical distance d_A, while keeping the net valence fixed [21]. Additionally, the entire doping range can be spanned from undoped to overdoped for all values of x. Therefore, x tunes both J (through a and θ) and orbital splitting (through d_A) over the whole phase diagram. Moreover, disorder in CLBLCO was found to be x independent based on the linewidths measured by techniques ranging from high-resolution powder x-ray diffraction [22], Cu, Ca, and O nuclear magnetic resonance [23–26], phonon [27], and angle-resolved photoemission spectroscopy (ARPES) [28].

Intriguingly, both J, as measured in undoped CLBLCO samples, and $T_c^{\max}$ were found to increase with x by as much as 40%. In fact, the energy scale of the entire phase diagrams, including the magnetic, spin glass, and superconducting parts, scales with J [29,30]. Such scaling was attributed to a superconductivity governed by J [27–30]. However, J in the optimally doped samples and the possible effects of the apical

*keren@physics.technion.ac.il

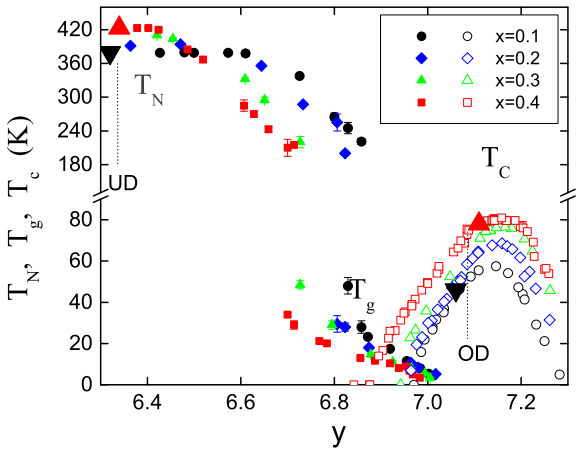

FIG. 1. (Color online) Phase diagram of CLBLCO obtained from powder samples in Ref. [29], which plots the Néel (T_N), spin-glass (T_g), and superconducting (T_c) transition temperatures as a function of the stoichiometric oxygen amount y for various families (x). The underdoped (UD), medium-doped (MD), and near-optimally doped (OD) single-crystal samples of the present study are placed in the diagram as black triangles (pointing down) for $x = 0.1$ and red triangles (pointing up) for $x = 0.4$.

oxygen distance are not known. Measuring those is the main objective of this work.

Recent milestones in the technique of resonant inelastic (soft) x-ray scattering (RIXS) have been the measurement of dispersive magnetic excitations in superconducting cuprates and iron pnictides [31–35]. This, together with single-crystal CLBLCO growths [36], have allowed us to measure how J varies with x in both underdoped and optimally doped CLBLCO samples. The momentum dependence provided by RIXS enables the precise determination of J based on the spin-wave dispersion. Fortuitously, the same probe is also sensitive to the orbital dd excitations [37]. Here we measure both effects simultaneously on CLBLCO single crystals. We also use x-ray absorption spectroscopy (XAS) to verify that the effective hole dopings are indeed the same when we compare families with different x.

We find that $T_c^{\max}$ has a positive, but not proportional, correlation with J. The $d_{xy} \rightarrow d_{x^2-y^2}$ and $d_{xz/yz} \rightarrow d_{x^2-y^2}$ splittings also increase with x, but we could not precisely isolate the $d_{3z^2-r^2} - d_{x^2-y^2}$ excitation. We nevertheless determine that in this system, ΔJ has a greater contribution (treating it as an independent variable) to the change in $T_c^{\max}$, compared to the out-of-plane orbital effect [13–18]. We also observe that the change in J is very similar in the undoped and doped samples, and the slope of the J-$T_c^{\max}$ relation is identical to that of YBCO under pressure. The RIXS spectra also reveal unexpected features, including a peak at 0.8 eV, and energy dispersive dd excitations.

The paper is organized as follows. Section II describes the experimental details. Presentation and analysis of the RIXS data are divided into the following sections: RIXS of underdoped samples, with focus on the spin excitations (Sec. III), RIXS of doped samples (Sec. IV), and dd or "crystal-field" orbital excitations (Sec. V). Section VI is a discussion of the context of these results and Sec. VII is the conclusion. Analysis of the doping from the O K-edge and Cu L-edge x-ray absorption spectra is provided in the Appendix.

II. EXPERIMENTAL DETAILS

$(Ca_xLa_{1-x})(Ba_{1.75-x}La_{0.25+x})Cu_3O_y$ single crystals were grown using the traveling float-zone method [36]. For each of $x = 0.1$ and $x = 0.4$, the underdoped (UD) samples (in y) were prepared by annealing in argon. The near-optimally doped (OD) samples were first annealed in flowing oxygen, followed by 100 Atm oxygen pressure for a period of two weeks. The oxygen content for the OD samples was confirmed by iodometric titration. The oxygen content for the UD sample was set based on the procedures used for powders so as to be in the antiferromagnetically long-range ordered phase [29]. The T_c's of the $x = 0.4$ and $x = 0.1$ OD samples were measured by magnetic susceptibility using a superconducting quantum interference device (SQUID) magnometer. They were 78 and 46 K, respectively, indicating a close to optimal doping condition. The place of the samples in the phase diagram is shown in Fig. 1.

Soft x-ray absorption spectroscopy (XAS) and RIXS measurements were conducted at the ADRESS beam line [38] at the Swiss Light Source of the Paul Scherrer Institut. The sample environment was ∼10 K in vacuum. The sample surfaces were cleaved c-axis faces, mounted such that the a (or equivalent b) axis was in the horizontal scattering plane. For XAS, to obtain incident polarization approximately parallel to the c axis, the sample was rotated to 10° from the grazing incidence condition. Refer to the Appendix for the detailed XAS results.

RIXS spectra were measured in the horizontal scattering plane. Measurements were done for both horizontally and vertically polarized incident beams, corresponding to π and σ polarizations, respectively. The incident energy was set to the first main peak in the Cu $L_{\rm III}$ XAS at 932 eV. The detector was fixed such that the two-θ scattering angle with respect to the incident beam was 130°. Throughout this paper, we refer to the in-plane momentum transfer q in reciprocal lattice units of $2\pi/a$, where a is the lattice constant of the crystal. We define q as the component of the total momentum change of the photon which is parallel to the sample ab plane [31]. Our sign convention is grazing incidence corresponding to negative q. The variation of a with each x [30] is accounted for in calculating q, but is not significant on the q scale. In our scattering configuration, q is always along the (1 0 0) direction, and its magnitude is changed by rotating the sample away from specular reflection. Therefore, the total momentum transfer is $\mathbf{Q} = (q,0,L)$ in tetragonal notation. The grazing incidence condition was used to calibrate the q position. This calibration was found to be valid by measuring E vs q dispersion for both positive and negative q (see Sec. III).

III. MAGNONS IN UNDERDOPED SAMPLES

Typical RIXS spectra for the UD samples are compared in Fig. 2 for $x = 0.1$ and $x = 0.4$. The various panels of Fig. 2 zoom in on different energy scales. The intensities are normalized to match at the strong dd peak in Fig. 2(b), and the energies are shifted so that the quasielastic peaks in

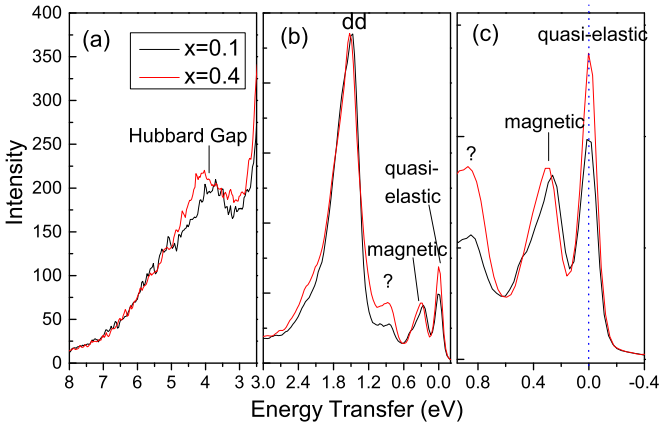

FIG. 2. (Color online) The main features of the typical CLBLCO RIXS spectra for $x = 0.1$ UD (black) and $x = 0.4$ UD (red) at various energy ranges: (a) 3–8 eV, (b) 0–3 eV, and (c) below 1 eV. In this example, the incident beam is π polarized and $q = -0.34$.

Fig. 2(c) are centered at zero. Figure 2(a) shows the relatively high-energy part of the spectra. First, we note that the $x = 0.1$ and $x = 0.4$ tails going down from 5 eV overlap closely. Second, there is a peak at around 4.5 eV which is in the energy range of charge-transfer excitations across the Hubbard gap. The feature is shifted to higher energy for $x = 0.4$ and is also present in the doped samples. A doping-independent feature at similar energy was studied in $La_{2-x}Sr_xCuO_4$ (LSCO) with Cu K-edge RIXS [39]. Figure 2(b) is an overall view of the spectra including both the intense peak encompassing the dd excitations between 1.5 and 1.8 eV and the lower energy peaks, which are much lower intensity but still visible on this scale. Comparison of the $x = 0.4$ and $x = 0.1$ spectra over a broad range reveals that generally, most of the excitations are at slightly higher energy for $x = 0.4$. This increased energy is ubiquitous both for the magnon excitations covered in this and the following section, and for the dd excitations in Sec. V. We note that both the high-energy tails in Fig. 2(a) and the quasielastic peaks in Fig. 2(c) are aligned in energy for the two samples. We will later show that the magnon and dd excitation-energy increases can be directly attributed to the change in lattice parameters.

Figure 2(c) zooms in on the low-energy range. At zero energy is a quasielastic peak, which depends on a combination of finite-q resolution of the instrument and the crystal mosaic of the sample. In our analysis, the energy scale of each spectra is shifted according to the center energy of the quasielastic peaks. In similar measurements done by Braicovich *et al.* [32] for La_2CuO_4, in which the quasielastic peak was much lower than it is here, a feature at around 80–90 meV was observed, with about a fifth of the magnon intensity. This was attributed to a resonantly enhanced optical phonon. We did not detect such a phonon and it is not included in our analysis.

The peak associated with magnons is found in the 0.2–0.4 eV range of Fig. 2(c). Comparison of the data for $x = 0.4$ (red) and $x = 0.1$ (black) clearly shows that the $x = 0.4$ peak is shifted to higher energy. Thus the main result that J is higher in the $x = 0.4$ sample than in the $x = 0.1$ samples is clearly evident already in the raw data.

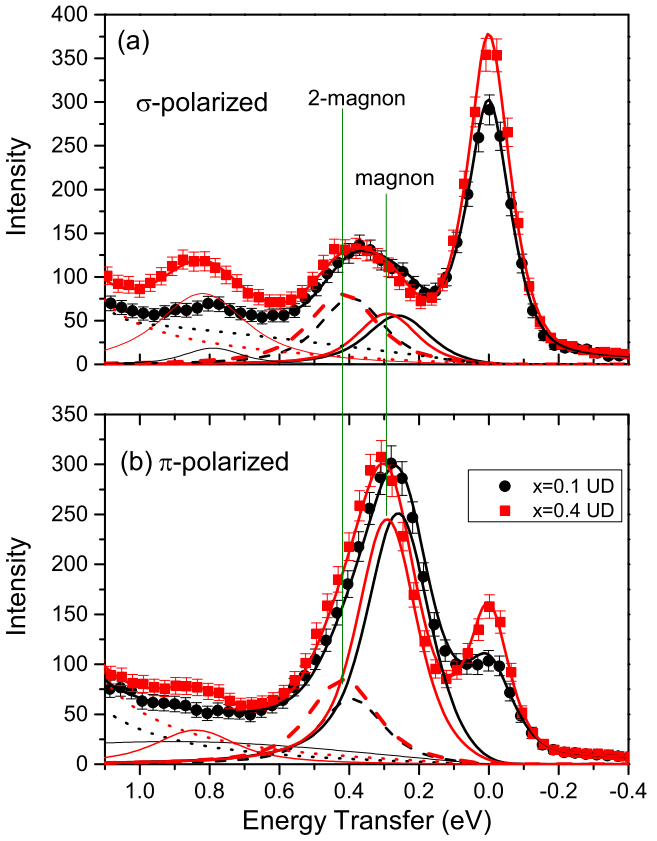

FIG. 3. (Color online) The RIXS spectra in underdoped samples at $q = 0.375$ for (a) σ- and (b) π-polarized configurations, corresponding to vertical and horizontal polarizations of the incident beam for scattering in the horizontal plane. The spectra of $x = 0.1$ (black) and $x = 0.4$ (red) samples are compared. The magnon (~0.25–0.3 eV) and two-magnon (~0.4 eV) component peaks are indicated as solid and dashed lines, obtained from simultaneous fitting of both (a) and (b) spectra. The dotted line shows a fit of the tail of the higher-energy dd excitation. A peak around 0.8 eV, much stronger in the $x = 0.4$ sample, is also present. The total fits are shown as solid lines crossing the data.

There is also a peak at ~0.8 eV. Its intensity is highest (comparable to the magnetic peak) at negative q for π-polarized scattering, but can be seen elsewhere (see Fig. 3) and is always stronger for the $x = 0.4$ sample. Where it is large, it was incorporated into our fitting for the magnons, described below. It has only slight dispersion of <0.05 eV, unlike the new mode recently observed by Lee *et al.* [40]. It would be surprising if the ~0.8 eV peaks were one of the three dd excitations, which are expected to be above 1.5 eV [41]. On the other hand, a dd excitation in the chain layer would be more plausible. Since half of the nonapical oxygen ligands around each Cu atom are missing in the chain, the Coulomb energy cost for a chain dd excitation should also be about half of a plane dd excitation, which corresponds to this ~ 0.8 eV.

A sample pair of spectra corresponding to the σ and π polarizations at the same q are shown in Figs. 3(a) and 3(b). To extract the magnon energies, fitting was done over the range shown in Fig. 3. Each spectrum was modeled as a sum of quasielastic peak, magnon peak, two-magnon peak, with

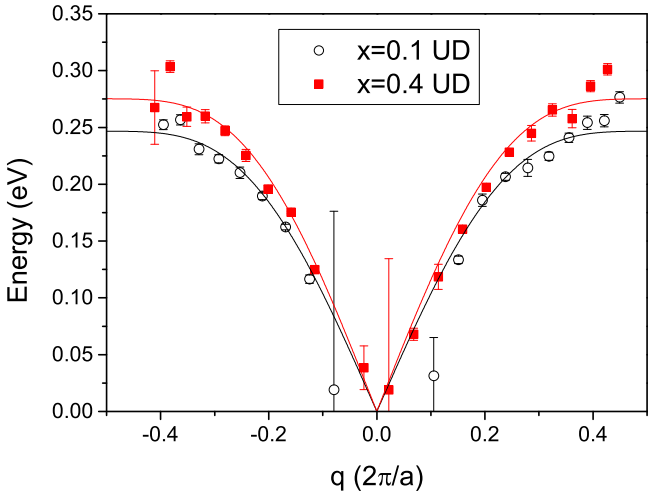

FIG. 4. (Color online) The dispersion along the (1 0 0) direction, of the fitted energies ν_R of the single-magnon components of the $x = 0.1$ (black) and $x = 0.4$ (red) UD samples. Fits to theoretical acoustic magnon dispersions of Ref. [43] for free parameter J, with $J_\perp$ fixed to 15 meV, are shown as black ($x = 0.1$) and red ($x = 0.4$) lines.

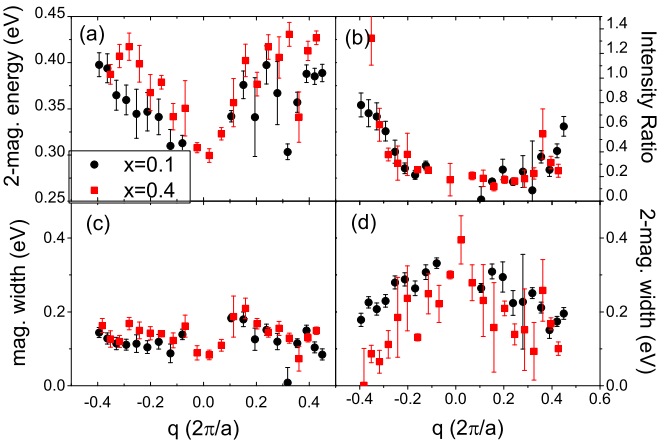

FIG. 5. (Color online) The other fit parameters for the $x = 0.1$ UD (black) and $x = 0.4$ UD (red) samples: (a) two-magnon energy, (b) ratio of two-magnon to magnon intensities in the π-polarized spectra, (c) intrinsic magnon width (FWHM), and (d) intrinsic two-magnon width.

(when visible) an additional peak at 0.8 eV, and a tail from the dd excitations. The spectral weight of the two-magnon peak relative to the magnon is generally different for the σ and π polarizations, resulting in a shift in the peak energy for the different polarizations. As in Ref. [33], the fitting is done for both polarizations simultaneously. The energies and widths of the magnon and two-magnon peaks were constrained to be the same for both polarizations, as indicated by the vertical lines in Fig. 3. The line shapes as a function of energy ν used for all of the excitations were a damped harmonic-oscillator response in the form of a Lorentzian, weighted according to "detailed balance":

$$S(\nu) = \frac{1}{1 - e^{-\nu/k_B T}} \times \left[\frac{(\Gamma/2)^2}{(\nu - \nu_R)^2 + (\Gamma/2)^2} - \frac{(\Gamma/2)^2}{(\nu + \nu_R)^2 + (\Gamma/2)^2} \right], \quad (1)$$

where T is the sample temperature, k_B is Boltzmann's constant, and fit parameters ν_R and Γ are the energy and intrinsic width, respectively. Each $S(\nu)$ was then convolved with a Gaussian representing the resolution function of the spectrometer to produce the components shown in Fig. 3. The fits for all spectra (more than 80) were excellent and are shown in the Supplemental Material [42]. The dispersion of ν_R for the magnon components is plotted in Fig. 4. The horizontal q axis for each sample was corrected by a slight shift (0.013 for $x = 0.1$ and 0.022 for $x = 0.4$) to make each dispersion symmetrical about the origin.

The dispersions are fit to a theoretical expression for acoustic-mode dispersion in the double-layer cuprate YBCO [43]:

$$E = 2J\{1 - \gamma^2(q) + (J_\perp/2J)[1 - \gamma(q)]\}^2 \quad (2)$$

for in-plane magnetic exchange J, with interplane coupling $J_\perp$ set to 15 meV, and $\gamma(q) = 0.5[\cos(2\pi q) + 1]$. There is also, in principle, an optical mode [43], but it resides quite close to the acoustic mode, except at low q, where the error bars are high. In our fitting, $J_\perp$ was fixed at 15 meV (which is similar to YBCO [43]), so the only free parameter was J. The fits are shown as the lines in Fig. 4. Equation (2) captures the nonlinearity of the data, particularly well on the negative-q side. The resultant J values were 134 ± 1 meV for $x = 0.4$ and 120 ± 1 meV for $x = 0.1$.

These values should be compared with the detailed *ab initio* calculations done by Petit and Lepetit for optimally doped CLBLCO [45]. Those yielded mean values of $J = 132$ meV for $x = 0.4$ and $J = 110$ meV for $x = 0.1$. The $x = 0.4$ results are in excellent agreement between theory and experiment, while there is a 10 meV difference for $x = 0.1$. We show in the next section that the dispersion of the UD and OD samples are similar.

The other fit parameters are plotted in Figs. 5(a)–5(d). In Fig. 5(a), the two-magnon energies at low q are close to 0.3 eV. This magnitude is within the range of the recent two-magnon Raman study in this material by Wulferding *et al.* [27], who measured energies of 0.29–0.35 eV in various samples. In addition, the sign and magnitude of dispersion of the two-magnon energy of about 0.1 eV in Fig. 5(a) is reasonably consistent with the ~80 meV measured with O K-edge RIXS by Bisogni *et al.* [44] in La_2CuO_4 (see Fig. 6 of Ref. [44]). Figure 5(b) plots the ratio of the intensities of the two-magnon to the one-magnon components. They fall on the same curve for $x = 0.1$ and $x = 0.4$, which is expected since the excitations in both should have the same symmetries.

Figures 5(c) and 5(d) show the intrinsic widths Γ for the magnon and two-magnon energies, which are 100–150 and >300 meV, respectively. These are wider than expected. The two-magnon widths observed in the Raman study [27] were only ~100 meV, while the magnon width is expected to be resolution limited on this scale. It is not clear if the large width originates in the fitting or sample. There is some intrinsic disorder in the site occupation between Ca, Ba, and La atoms, which could be a potential cause of an intrinsic

magnon width. But if so, we note that the widths of $x = 0.1$ and $x = 0.4$ are about the same, indicating that x does not affect disorder. Nevertheless, our analysis (i) fit all of the data excellently with minimal number of parameters, (ii) resulted in a realistic dispersion curve with J values which are in good agreement with Ref. [45], and (iii) two-magnon energies at low q are consistent with the two-magnon energies measured with Raman scattering [27], and (iv) two-magnon dispersion is consistent with O K-edge value for La_2CuO_4 from Ref. [44].

IV. PARAMAGNONS OF OPTIMALLY DOPED SAMPLES

Here we estimate the change in J in the superconducting samples. For doped cuprates, Le Tacon *et al.* found that the lifetime broadening of the spin excitations makes the widths too broad to distinguish between magnon and two-magnon peaks, and instead they are replaced by a single "paramagnon" peak [33]. A typical spectrum for the OD CLBLCO samples is shown in Fig. 6. As in Ref. [33], we replaced the magnon and two-magnon peak with a single magnetic component, retaining the line shape of Eq. (1). Only the elastic intensity, paramagnon peak, and the tail from the dd were included in the fits. Most of the q's measured were positive and there were no strong 0.8 eV peaks. Since the peak position is generally different for π and σ polarizations, due to different weights of the two-magnon and magnon contributions (as seen in Fig. 3), both could not be fit simultaneously with one peak. We therefore chose to use only the π polarization. The single peak of Eq. (1) plus background fit quite well to the data; fits to all of the spectra are shown in the Supplemental Material [42]. As seen in both the fits and raw data of Fig. 6, the paramagnon for $x = 0.4$ is shifted with respect to $x = 0.1$ and extends to higher energy, which was also typical for the other q's. We note that in Fig. 6, the dd tails from high energy are the same for $x = 0.1$ and $x = 0.4$.

A series of spectra for progressively higher q are plotted in Fig. 7(a) for the UD samples and in Fig. 7(b) for the

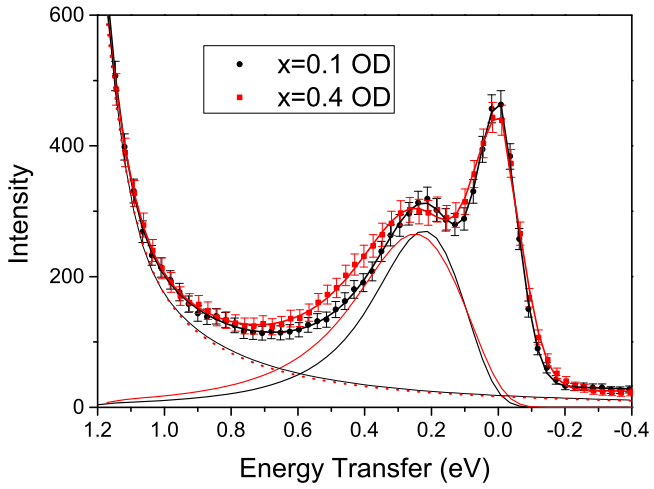

FIG. 6. (Color online) π-polarized spectra of $x = 0.1$ (black) and $x = 0.4$ (red) OD samples, at $q = 0.266$. The fit of the magnetic component to an asymmetric Lorentzian plus background, and the magnetic peak component itself, are shown as lines with the same color code. The high-energy dd tail of $x = 0.4$ closely coincides with that of $x = 0.1$, and is shown as a dotted line.

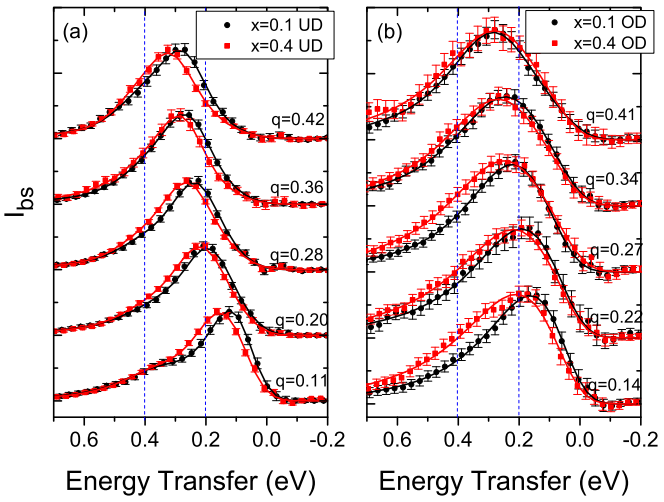

FIG. 7. (Color online) Comparison of the background-subtracted spectral intensity (I_{bs}) between (a) UD and (b) OD samples measured at similar q positions. The spectra were obtained by subtracting the quasielastic dd and 0.8 eV fitted components (if present) from the π-polarized spectra. The dashed vertical lines are guides for the eye.

OD samples. The spectra in Fig. 7(a) for the UD samples were obtained by subtracting all of the fitted components (see Sec. III) from the raw data, save for the magnon and two-magnon contributions. The same procedure is applied to the OD samples in Fig. 7(b), by subtracting the nonmagnetic contribution. The q positions are similar for Figs. 7(a) and 7(b). Both pairs of spectra in Figs. 7(a) and 7(b) are centered below 0.2 eV at low q (bottom spectra), and by $q = 0.4$ (top spectra) they dispersed to 0.3 eV. This similarity suggests that the J comparison for the UD spectra, which is generally easier to precisely determine, is also valid for the superconducting case. It also would seem to argue against the scenario of intraband excitations (as opposed to paramagnons) which was recently proposed by Benjamin *et al.* [46], since the OD and UD spectra have the same energies.

The value of J cannot directly be determined from the paramagnon spectra. The fitted energy parameter ν_R of the asymmetric line shape in Eq. (1) does not have the same well-defined meaning as in the two-peak, two-polarization fits used in Sec. III. This is because the peak fitted for here encompasses both magnon and two-magnon components, weighted by some unknown amount depending on the scattering cross section for each [one can refer to Fig. 5(b) for the UD case]. Instead, for comparison purposes, we use the center of mass, namely, the statistical mean energy $\langle E_M \rangle = \frac{\int E \cdot I_{bs}(E) dE}{\int I_{bs}(E) dE}$ of the background-subtracted magnetic spectra $I_{bs}(E)$ of Fig. 7(b). While this definition is arbitrary, for a given q, it should be roughly proportional to J for any two samples, since both magnon and two-magnon energies are proportional to J.

$\langle E_M \rangle$ is plotted as a function of q in Fig. 8 for $x = 0.1$ (black circles) and $x = 0.4$ (red squares). For all but the last, it is higher for $x = 0.4$. The average over these q points, $\overline{\langle E_m \rangle}$, is 0.33 eV for $x = 0.1$ and 0.36 eV for $x = 0.4$. Assuming proportionality, we interpret this as a 9% increase in J from $x = 0.1$ to $x = 0.4$. By comparison, the percentage increase for the (more precisely determined) J's of the UD samples

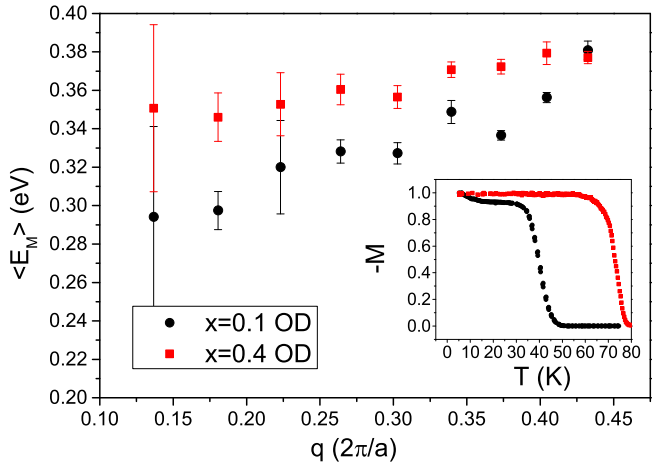

FIG. 8. (Color online) The dispersion of the energy center of mass $\langle E_M \rangle$ of the magnetic peak of the OD samples as described in the text. To emphasize their T_c variations, the inset shows the magnetization vs temperature of the two samples, normalized to their maximum diamagnetic responses at low temperature.

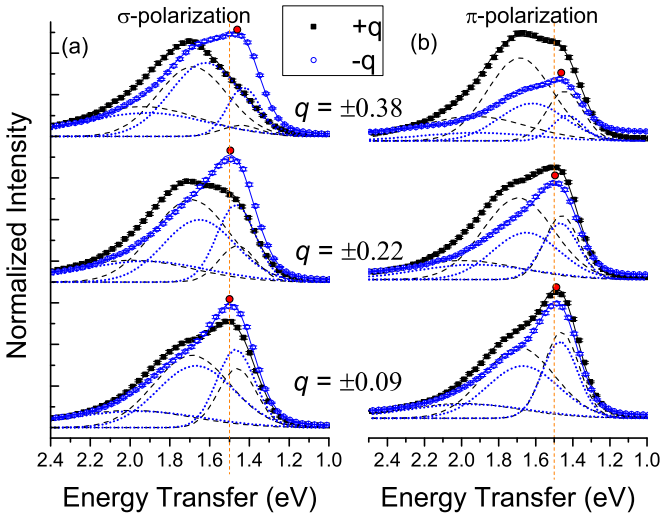

FIG. 9. (Color online) dd spectra of the UD sample for $x = 0.1$ at representative q positions for (a) σ polarization and (b) π polarization. The three Gaussian components are indicated as dashed/dotted lines and the total fit as solid lines. The filled black squares/dashed lines correspond to positive q, and the empty blue circles/dotted lines correspond to negative q (closer to grazing incidence). The vertical lines and red circles are guides for the eye.

in Sec. III is 11.7%. Considering the broad widths of the OD spectra and the somewhat cruder method of estimating their ΔJ, this estimated increase is quite close to the UD case.

In the inset of Fig. 8, we present the negative magnetization measurements of the two superconducting samples used for RIXS. There is a clear difference in their T_c. The main observation of this work is that the sample with higher T_c also has higher J. It was also demonstrated here that RIXS can distinguish samples with small differences in J even in the optimally doped case.

V. CRYSTAL-FIELD (dd) EXCITATIONS

The dd spectra of our UD samples were generally sharper than for our OD samples, so we focus on the former. The dd excitation spectra of the UD samples are plotted in Fig. 9 for selected q 's for the $x = 0.1$ sample. The spectra of the $x = 0.4$ sample was qualitatively similar in the main features, but with slightly higher energies [see Fig. 2(b)]. All of the spectra and fittings for the full range of q's are presented in the Supplemental Material [42]. The centering of the quasielastic peaks of all of the spectra is also shown in the Supplemental Material to be accurate within ∼10 meV. At least two peaks are clearly resolved, at ∼1.5 and ∼1.7 eV, with the intensity of the 1.7 eV peak becoming relatively stronger with increased q. We fit the π- and σ-polarized spectra simultaneously to a sum of Gaussians, constraining the parameters of widths and energies to be the same for both polarizations. Three Gaussians worked best. They are shown in Fig. 9. The zero energies are defined by the elastic peaks (see Sec. III). As can be seen in Fig. 9, the widths successively increased from the low- to high-energy peaks.

To assign the peaks, we refer to the work of Sala *et al.* [41], who studied dd excitations with Cu L-edge RIXS in a variety of cuprates. They found excellent agreement between the observed polarization and q dependence, and their cross-section calculations. The compound studied in that work, which is structurally similar to CLBLCO, is the double-layer 123-cuprate $NdBa_2Cu_3O_7$ (NBCO). In what follows, E_{xy}, $E_{xz/yz}$, and $E_{3z^2-r^2}$ refer to the energies of the orbital transitions $d_{xy} \rightarrow d_{x^2-y^2}$, $d_{xz/yz} \rightarrow d_{x^2-y^2}$, and $d_{3z^2-r^2} \rightarrow d_{x^2-y^2}$, respectively. The NBCO spectra had two prominent peaks at 1.52 and 1.75 eV, which the authors of Ref. [42] assigned to E_{xy} and $E_{xz/yz}$. $E_{3z^2-r^2}$ was calculated to be 1.97 eV, but it was not visible in their spectra. As q increased, the cross section of the 1.75 eV peak increased relative to the 1.5 eV peak. These results, both the energies and cross-section q dependence, are very close to what we observe for CLBLCO in Fig. 9. We therefore likewise assign the 1.5 eV peak to E_{xy} and the 1.7 eV peak to $E_{xz/yz}$. Furthermore, the energy of the broad third Gaussian component in Fig. 9 happened to lie very close to 2 eV, with zone averages (standard deviations) of 1.97(0.03) and 2.00(0.1) eV for $x = 0.1$ and $x = 0.4$, respectively. While this energy is in excellent agreement with calculations for $E_{3z^2-r^2}$ in NBCO [41] and for YBCO [47], the broadness makes it difficult to identify with certainty.

The q dependence of E_{xy} and $E_{xz/yz}$ is plotted in Fig. 10 for $x = 0.1$ and $x = 0.4$. Surprisingly, there appears to be some dispersion in the energies. The d_{xy} excitation for $x = 0.1$ shows flat dispersion near the zone center, up to around $|q| = 0.2$, but beyond this it exhibits negative dispersion of the order of 0.05 eV towards the zone boundary. This E_{xy} dispersion is quite symmetrical about $q = 0$, up to $q = 0.35$. The dispersion could also be seen from the raw data. In Fig. 9, the red circles mark the low-energy peaks of the negative-q branch. They also mark the positive branch, but it is harder to see for high $|q|$, especially for σ polarization. For the bottom two spectra, corresponding to $|q| = 0.09$ and $|q| = 0.22$, the peaks are aligned with the vertical dashed line, but by $|q| = 0.38$, the peak of the raw data is visibly shifted to the right of the line by about 50 meV. A nonzero dispersion suggests propagation of the orbital excitation. For $x = 0.4$, the d_{xy} excitation shows similar dispersion on the negative branch, but its magnitude

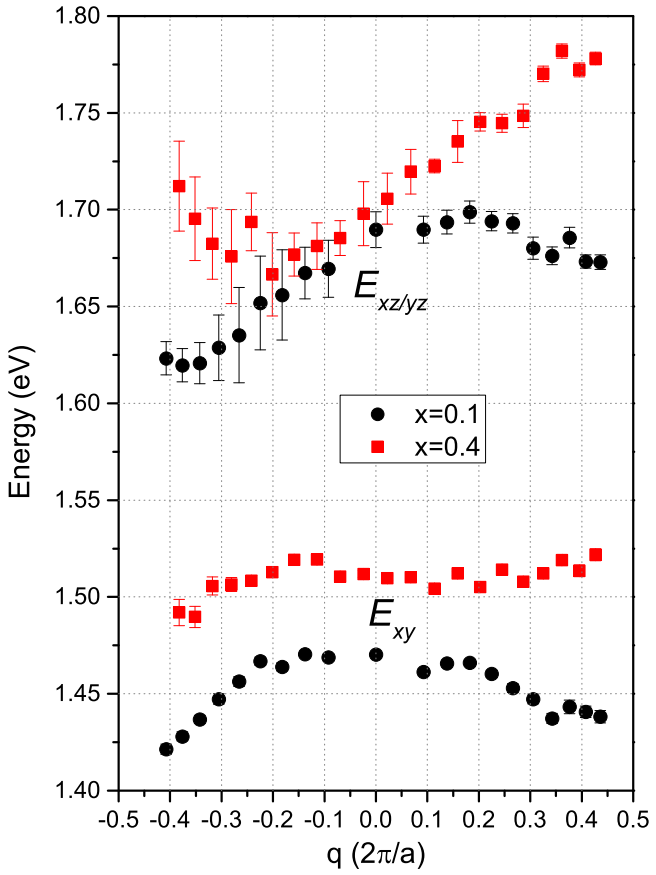

FIG. 10. (Color online) The fitted dd energies E_{xy} and $E_{xz/yz}$ which resulted from the simultaneous fitting to both π and σ polarizations, plotted for each q position. The energies of $x = 0.1$ (black) and $x = 0.4$ (red) are plotted.

is roughly halved. $E_{xz/yz}$ also shows dispersion, but is not symmetrical about $q = 0$. The fitted energies for $x = 0.4$ especially show a linear trend with a dispersion of almost 0.1 eV between $q = \pm 0.2$. Unlike the E_{xy} dispersion, the $E_{xz/yz}$ dispersion is not obvious from the raw data itself due to the wider peaks, and only becomes apparent after the fittings. Although it seems counterintuitive, asymmetric dispersion may happen in the presence of spin-orbit interaction. It has already been observed in the spin wave of Fe ultrathin films [48], for example. Whether similar asymmetry can exist in the dispersion of an orbital excitation, as suggested by the present fits, is beyond the scope of this paper.

We can check whether E_{xy} scales properly with the lattice parameter. As pointed out by Sala *et al.* [41], $E_{xy} \propto a^{-n}$. Averaging the energies of Fig. 10 over the zone yields, for $x = 0.1$ ($x = 0.4$), $\overline{E}_{xy} = 1.46$ (1.52) and $\overline{E}_{xz/yz} = 1.69$ (1.75) eV. The corresponding a value for $x = 0.1$ is $a = 3.91$ Å and for $x = 0.4$ is $a = 3.88$ Å. This yields $n = 5.1$ remarkably close to the theoretical single-ion crystal-field model's value of $n = 5$.

VI. DISCUSSION

Analysis of the UD spectra in Sec. III provided explicit J values of 120 meV ($x = 0.1$) and 134 meV ($x = 0.4$). The corresponding $T_c^{\max}$ for these x values are 57 and 80 K, respectively [29]. In Sec. IV, we found that the change in J for doped samples is comparable to the undoped case, and the two dopings furthermore exhibit very similar dispersions of the spin-excitation spectra (refer to Fig. 7). It is therefore justified to apply the UD values of J to the superconducting case, as has been assumed to be valid in other works [7,27]. With x as an implicit parameter, we find that $\Delta T_c^{\max}/\Delta J = 1.64$ K/meV. This is the same order of magnitude of the average slope obtained from the study of Munoz *et al.* [5] of several cuprates having different numbers of layers (~3.2 K/meV). It is even more closely aligned with the initial slope for YBCO under hydrostatic pressure (~1.5 K/meV) [7]. Moreover, the increase of J of 11.7% from $x = 0.1$ to $x = 0.4$ determined for the UD samples in Sec. III is in close agreement with the estimation of 11.9% we obtain by using a simple $J \propto \cos^2\theta/a^{14}$ rule [30]. In addition, E_{xy} scales as expected with distances. These results indicate that the in-plane energies $J(x)$ and $E_{xy}(x)$ depend purely on in-plane parameters, without secondary effects arising from different Ca/Ba ratios. We speculate that the $d_{3z^2-r^2} \rightarrow d_{x^2-y^2}$ peak, which we could not properly resolve, behaves as expected from the lattice parameters variations between different CLBLCO families.

Whether $T_c^{\max}(x)$ likewise depends only on the in-plane parameters is not *a priori* clear, since the out-of-plane lattice parameter c and apical oxygen distance d_A are also functions of x. In fact, a number of studies [13–18,49] focused on the effect of d_A and $E_{3z^2-r^2}$ on $T_c^{\max}$ in various cuprate systems. We now assess the relative importance that these have for $T_c^{\max}(x)$.

Since YBCO and CLBCO share very similar structure and lattice parameters, it is relevant to compare the two. The values of $\Delta T_c^{\max}/\Delta J$ observed in the pressure dependence of YBCO, on one hand, and in the x dependence of CLBLCO observed here, on the other hand, are very similar. Hydrostatic pressure compresses the c axis, decreasing the apical oxygen distance d_A and increasing T_c. In contrast, when increasing x (and $T_c^{\max}$) in CLBLCO, d_A increases [30]. That $\Delta T_c^{\max}/\Delta J$ is the same for YBCO and CLBLCO, in spite of d_A changing in the opposite sense, leads us to conclude that d_A variations do not play a major role here in determining $T_c^{\max}$.

Another way to reach this conclusion for CLBLCO is to estimate the effect of the change in d_A on $T_c^{\max}$ by comparing with other studies. A sensitivity of roughly $\frac{\partial T_c^{\max}}{\partial d_A} \sim 30$ K/Å, was shown across various cuprates by Johnston *et al.* [49] (see Fig. 1 of Ref. [49]). In CLBLCO powder, as x increases from 0.1 to 0.4, d_A increases by ~0.05 Å [30]. On that basis, the effect of Δd_A on T_c in CLBLCO would be less than 2 K.

A similar effect of Δd_A on T_c results from the theoretical calculations of $E_{3z^2-r^2}(d_A)$ by Sakakibara *et al.* [15]. They calculated the Eliashberg eigenvalue λ which sets a limit on T_c. From their calculations, an upper limit of $\frac{\partial T_c^{\max}}{\partial d_A} < 125$ K/Å can be set, which is still too small to account for the T_c variations in CLBLCO.

Taken together, the above comparisons suggest that Δd_A in CLBLCO has very little impact on $T_c^{\max}$. By eliminating this out-of-plane influence, it becomes more likely that the change in $T_c^{\max}$ observed between different families of CLBLCO is due to variations in J. While $T_c^{\max}$ increases by 40% (Fig. 1) from $x = 0.1$ to $x = 0.4$, J as measured by RIXS only

increases by ∼11.7%. From other methods, the corresponding increase in J for samples with the same in-plane hole underdoping was determined to be 21% from the two-magnon Raman peaks [27], 26% from angle-resolved photoemission spectroscopy [28], 20% in *ab initio* calculations [45], and 40% by μSR with extraction of J from T_N [29]. With the exception of the latter, these estimates were all considerably less than the increase in $T_c^{\max}$. This suggests that the J dependence of T_c is not proportional, as predicted by some exchange-driven theories [3,4]. If a linear relationship extends down to $T_c^{\max} = 0$, it would imply a threshold J for superconductivity.

VII. CONCLUSION

To review, we measured the O K-edge and Cu L-edge XAS, and RIXS spectra at the Cu L-edge, in both underdoped and optimally doped CLBLCO single crystals of $x = 0.1$ and $x = 0.4$ families which have different $T_c^{\max}$.

From the electronic structure of the XAS spectra, similar hole dopings in the superconducting samples of the different families were confirmed. As it turns out, doping does not have a critical effect on the magnon dispersion, besides a broadening of the peaks. The relative change in magnetic energies between $x = 0.1$ and $x = 0.4$ are furthermore similar for the doped and undoped cases. This demonstrates that RIXS can distinguish between samples of slightly different J even in the doped case.

The main dd excitations were also examined and unexpectedly dispersion of up to 0.05 eV was observed, raising the possibility that these orbital excitations can propagate. More intriguingly, the dispersion of the excitation from the $d_{xz/yz}$ orbit appeared to be asymmetric about $q = 0$. Higher-resolution studies would be needed to clarify this dispersion. In the UD samples, an additional 0.8 eV peak was observed and attributed to a dd excitation in the chain layer.

Finally, there is a positive correlation between $T_c^{\max}$ and J with a slope consistent with the pressure dependence of both parameters in YBCO. The measured spin-wave energies change with x by an amount that would be expected from a purely in-plane lattice-constant change. Furthermore, it is concluded that the apical oxygen distance does not change enough with x to have a significant effect on $T_c^{\max}$. These points suggest that the $T_c^{\max}$ variation with x in CLBLCO is purely an in-plane effect driven by orbital overlaps.

ACKNOWLEDGMENTS

The RIXS and XAS measurements were performed on the ADRESS beam line at the Swiss Light Source, Paul Scherrer Institut, Villigen, Switzerland. Part of this work has been funded by the Swiss National Science Foundation and its Sinergia Network Mott Physics Beyond the Heisenberg (MPBH) model. J.P. and T.S. acknowledge financial support through the Dysenos AG by Kabelwerke Brugg AG Holding, Fachhochschule Nordwestschweiz, and the Paul Scherrer Institut. We acknowledge financial support from the Israel Science Foundation Grants No. 249/10 (J.B. and D.E.) and No. 666/13 (G.D., R.O., G.B., and A.K.). The research leading to these results has received funding from the European Community's Seventh Framework Programme (FP7/2007-2013) CALIPSO under Grant No. 312284. We also thank Daniel Podolsky for helpful discussions.

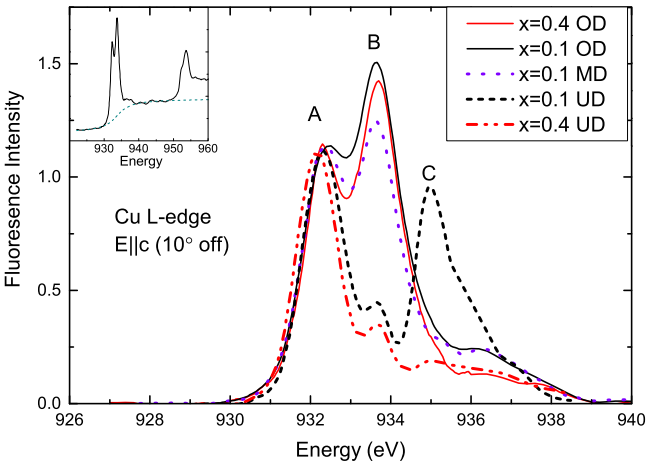

FIG. 11. (Color online) The x-ray absorption spectra at the copper $L_{\rm III}$ edge, after background subtraction, for the four CLBLCO samples, $x = 0.4$ and $x = 0.1$ optimally (OD) doped and underdoped (UD) samples, and an additional $x = 0.1$ sample at medium doping (MD). The electric field was aligned 10° from the c axis. The three main peaks are labeled A, B, and C. Inset: An example fitting of the background.

APPENDIX: XAS ANALYSIS

In addition to determining the resonance energy needed for RIXS, XAS also provides valuable information about the number of holes present in our samples. We measured the XAS of the single crystal $x = 0.4$ OD and UD and $x = 0.1$ OD and UD samples. In addition, an $x = 0.1$ sample of intermediate doping (MD), estimated to be just before the onset of superconductivity, was measured. We used much of the same approach for analysis as was used by Agrestini *et al.* [22] for treatment of CLBLCO powder. The clearest and most systematic spectra were at the Cu $L_{\rm III}$ edge when the electric

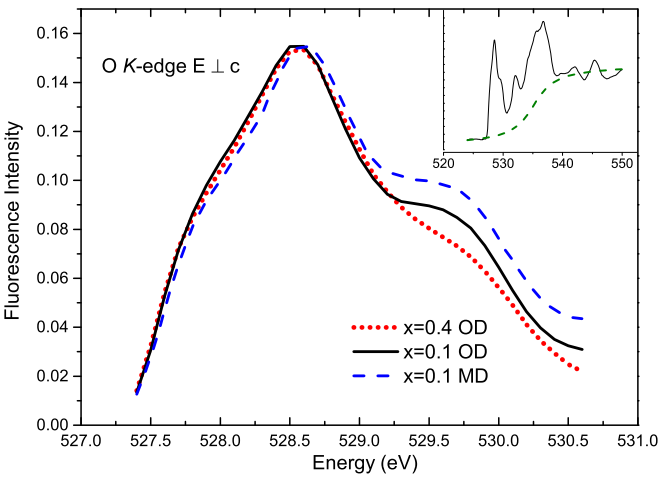

FIG. 12. (Color online) XAS at the oxygen K edge after background subtraction, with electric field parallel to the ab plane. The data were normalized to have the same maximum intensity.

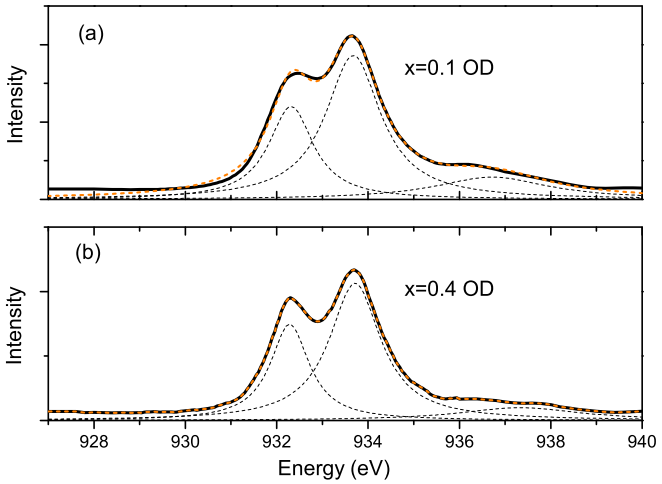

FIG. 13. (Color online) Fitting of the background-subtracted XAS spectra to three Lorentzians for the optimally doped samples for (a) $x = 0.1$ and (b) $x = 0.4$.

field is polarized along the c axis (with a 10° misalignment from axis), and at the O K-edge absorption when the electric field is polarized parallel to the ab plane. These are shown in Figs. 11 and 12, respectively, after subtracting a background in the form of an inverse tangent function, as shown in the insets. Referring to Fig. 11, the data were normalized so as to have the same maxima of peak A for all samples, which comes from the Cu $3d^9 \rightarrow$ Cu $2\bar{p}3d^{10}$ transition [22,50].

The low-energy edges of the A peaks of all samples match perfectly, with the exception of $x = 0.4$ UD, whose A peak is shifted to slightly lower energy. The second peak B is at the same energy for all samples. It corresponds to the same absorption process as A, but in the presence of a ligand hole, namely, Cu $3d^9\bar{L} \rightarrow$ Cu $2\bar{p}3d^{10}\bar{L}$ [22,50]. It is clear that peak B becomes less and less intense as the doping decreases, but is roughly the same between $x = 0.1$ and $x = 0.4$ for identical nominal dopings. A third peak C appears for the UD samples ~3 eV from peak A. It is quite strong for $x = 0.1$, but is only a small bump for $x = 0.4$. Such a peak is associated with charge-transfer excitations to the upper Hubbard band [51,52]. A satellite peak around that energy has been related to the chain layer in the 123 compounds [53].

The number of holes can be determined from the relative B peak intensity [22,54]. The spectra were fitted to three Lorentzians, as shown in Fig. 13 for the OD samples. The ratio of the areas of the components, $B/(A + B)$, for OD $x = 0.4$ and $x = 0.1$ samples was 0.652 ± 0.01 and 0.657 ± 0.01, respectively, indicating identical hole doping for both samples. Additionally, we can estimate y and the total number of holes in a unit cell including chains and planes, h. Roughly 20% of h is expected to be in each plane [50]. From the measured T_c of the OD samples, combined with the phase diagram for powders (see Fig. 1) [30], we obtain $y = 7.06$ and 7.11 for the $x = 0.4$ and $x = 0.1$ samples, respectively. This is near the top but slightly to the left of the peak of the superconducting domes. We then estimate the amount of holes using the relation $h = y - 6.25$ [22]. Using that as a reference and assuming the $B/(A + B)$ area ratios are proportional to h, we can estimate h and y of the UD and MD samples. Table I is a summary of the intensity ratios, estimated h, and the various samples, estimated y. We note that $y_{UD} \simeq 6.32$–6.34, placing it well into the antiferromagnetic long-range ordered phase (Fig. 1). Likewise, $y_{MD} \simeq 6.94$, which is consistent with the iodometric titration result of 6.92 for this sample.

TABLE I. Table of parameters determined from the Cu L-edge absorption spectra. The columns are the sample, relative area of the B peak, estimated total number of holes h, and estimated oxygen content y. As described in the text, for the first two rows, y was estimated based on T_c, and then h was calculated. In subsequent rows, h was calculated first, followed by y.

Sample	$B/(A + B)$	h	y
$x = 0.4$ OD	0.652 ± 0.01	0.86	7.11
$x = 0.1$ OD	0.657 ± 0.01	0.81	7.06
$x = 0.1$ MD	0.561 ± 0.02	0.69	6.94
$x = 0.1$ UD	0.055 ± 0.02	0.07	6.32
$x = 0.4$ UD	0.067 ± 0.01	0.09	6.34

To further compare the relative hole densities, the normalized oxygen K-edge spectra is plotted in Fig. 12. It was measured for the $x = 0.1$ OD, $x = 0.4$ OD, and $x = 0.1$ MD samples. The effect of the holes may be seen by inspection of the positions of the low-energy peak of the O K-edge spectra. Shifts in this oxygen "pre-edge" energy track the shift in Fermi level with hole doping [50,54]. This shift is a direct consequence of the filling (or emptying) of the bands. From Fig. 12, the low-energy oxygen K edges overlap almost exactly for the $x = 0.4$ and $x = 0.1$ OD samples. In contrast, the edge of the $x = 0.1$ MD spectrum shifts by about 0.07 eV. Based on the result shown for YBCO in Ref. [50], the shift would correspond to a change in doping of $\delta y \simeq 0.20$. This is of the same order of magnitude as $\delta y \simeq 0.12$ between the OD and MD samples in Table I. The almost overlapping edges for the $x = 0.1$ and $x = 0.4$ OD samples is therefore a second confirmation of identical number of holes, and furthermore indicates that the amount of holes in the plane layer is the same.

[1] D. J. Scalapino, Rev. Mod. Phys. **84**, 1383 (2012).
[2] P. W. Anderson, Science **235**, 1196 (1987).
[3] D. J. Scalapino and S. R. White, Phys. Rev. B **58**, 8222 (1998).
[4] O. P. Sushkov and V. N. Kotov, Phys. Rev. B **70**, 024503 (2004).
[5] D. Muñoz, F. Illas and I. de P. R. Moreira, Phys. Rev. Lett. **84**, 1579 (2000).
[6] D. Muñoz, I. de P. R. Moreira, and F. Illas, Phys. Rev. B **65**, 224521 (2002).
[7] B. P. P. Mallett, T. Wolf, E. Gilioli, F. Licci, G. V. M. Williams, A. B. Kaiser, N. W. Ashcroft, N. Suresh, and J. L. Tallon, Phys. Rev. Lett. **111**, 237001 (2013).
[8] M. P. M. Dean, A. J. A. James, A. C. Walters, V. Bisogni, I. Jarrige, M. Hücker, E. Giannini, M. Fujita, J. Pelliciari, Y. B.

Huang, R. M. Konik, T. Schmitt, and J. P. Hill, Phys. Rev. B **90**, 220506(R) (2014).
[9] M. W. McElfresh, M. B. Maple, and K. N. Yang, Appl. Phys. A **45**, 365 (1988).
[10] N. Mori, C. Murayama, H. Takahashi, H. Kaneko, K. Kawabata, Y. Iye, S. Uchida, H. Takagi, Y. Tokura, Y. Kubo, H. Sasakura, and K. Yamaya, Physica C **185–189**, 40 (1991).
[11] S. Koltz, W. Reith, and J. S. Schilling, Physica C **172**, 423 (1991).
[12] S. Sadewasser, J. S. Schilling, A. P. Paulikas, and B. W. Veal, Phys. Rev. B **61**, 741 (2000).
[13] Y. Ohta, T. Tohyama, and S. Maekawa, Phys. Rev. B **43**, 2968 (1991).
[14] E. Pavarini, I. Dasgupta, T. Saha-Dasgupta, O. Jepsen, and O. K. Andersen, Phys. Rev. Lett. **87**, 047003 (2001).
[15] H. Sakakibara, H. Usui, K. Kuroki, R. Arita, and H. Aoki, Phys. Rev. Lett. **105**, 057003 (2010).
[16] K. Kuroki, J. Phys. Chem. Solids **72**, 307 (2011).
[17] H. Sakakibara, H. Usui, K. Kuroki, R. Arita, and H. Aoki, Phys. Rev. B **85**, 064501 (2012).
[18] R. Yoshizaki, T. Yamamoto, H. Ikeda, and K. Kadowaki, J. Phys. Conf. Ser. **400**, 022142 (2012).
[19] S. Raghu, R. Thomale, and T. H. Geballe, Phys. Rev. B **86**, 094506 (2012).
[20] D. Goldschmidt, G. M. Reisner, Y. Direktovitch, A. Knizhnik, E. Gartstein, G. Kimmel, and Y. Eckstein, Phys. Rev. B **48**, 532 (1993).
[21] S. Sanna, S. Agrestini, K. Zheng, R. de Rezni, and N. L. Saini, Europhys. Lett. **86**, 67007 (2009).
[22] S. Agrestini, S. Sanna, K. Zheng, R. de Renzi, E. Psuceddu, G. Concas, N. L. Saini, and A. Bianconi, J. Phys. Chem. Solids **75**, 259 (2014).
[23] S. Marchand, Ph.D. thesis, Université Paris, 2005.
[24] A. Keren, New J. Phys. **11**, 065006 (2009).
[25] E. Amit and A. Keren, Phys. Rev. B **82**, 172509 (2010).
[26] T. Cvitanić, D. Pelc, M. Požek, E. Amit, and A. Keren, Phys. Rev. B **90**, 054508 (2014).
[27] Dirk Wulferding, Meni Shay, Gil Drachuck, Rinat Ofer, Galina Bazalitsky, Zaher Salman, Peter Lemmens and Amit Keren, Phys. Rev. B **90**, 104511 (2014).
[28] G. Drachuck, E. Razzoli, R. Ofer, G. Bazalitsky, R. S. Dhaka, A. Kanigel, M. Shi, and A. Keren, Phys. Rev. B **89**, 121119(R) (2014).
[29] R. Ofer, G. Bazalitsky, A. Kanigel, A. Keren, A. Auerbach, J. S. Lord, and A. Amato, Phys. Rev. B **74**, 220508(R) (2006).
[30] R. Ofer, A. Keren, O. Chmaissem, and A. Amato, Phys. Rev. B **78**, 140508 (2008).
[31] L. Braicovich, L. J. P. Ament, V. Bisogni, F. Forte, C. Aruta, G. Balestrino, N. B. Brookes, G. M. De Luca, P. G. Medaglia, F. Miletto Granozio, M. Radovic, M. Salluzzo, J. van den Brink, and G. Ghiringhelli, Phys. Rev. Lett. **102**, 167401 (2009).
[32] L. Braicovich, J. van den Brink, V. Bisogni, M. M. Sala, L. J. P. Ament, N. B. Brookes, G. M. De Luca, M. Salluzzo, T. Schmitt, V. N. Strocov, and G. Ghiringhelli, Phys. Rev. Lett. **104**, 077002 (2010).
[33] M. Le Tacon, G. Ghiringhelli, J. Chaloupka, M. Moretti Sala, V. Hinkov, M. W. Haverkort, M. Minola, M. Bakr, K. J. Zhou, S. Blanco-Canosa, C. Y. T. Song, G. L. Sun, C. T. Lin, G. M. De Luca, M. Salluzzo, G. Khaliullin, T. Schmitt, L. Braicovich, and B. Keimer, Nat. Phys. **7**, 725 (2011).
[34] K-J. Zhou, Y-B. Huang, C. Monney, X. Dai, V. N. Stocov, N-L. Wang, Z-G. Chen, C. Zhang, P. Dai, L. Patthey, J. van den Brink, H. Ding and Thorsten Schmitt, Nat. Commun. **4**, 1470 (2013).
[35] M. P. M. Dean, G. Dellea, R. S. Springell, F. Yakhou-Harris, K. Kummer, N. B. Brookes, X. Liu, Y-J. Sun, J. Strle, T. Schmitt, L. Braicovich, G. Ghiringhelli, I. Bozovic, and J. P. Hill, Nat. Mater. **12**, 1019 (2013).
[36] G. Drachuck, M. Shay, G. Bazalitsky, R. Ofer, Z. Salman, A. Amato, C. Niedermayer, D. Wulferding, P. Lemmens, and A. Keren, J. Superconduct. Novel Magn. **25**, 2331 (2012).
[37] G. Ghiringhelli, N. B. Brookes, E. Annese, H. Berger, C. Dallera, M. Grioni, L. Perfetti, A. Tagliaferri, and L. Braicovich, Phys. Rev. Lett. **92**, 117406 (2004).
[38] V. N. Strocov, T. Schmitt, U. Flechsig, T. Schmidt, A. Imhof, Q. Chen, J. Raabe, R. Betemps, D. Zimoch, J. Krempasky, X. Wang, M. Grioni, A. Piazzalunga, and L. Patthey, J. Synch. Radiat. **17**, 631 (2009).
[39] D. S. Ellis, Jungho Kim, H. Zhang, J. P. Hill, G. Gu, S. Komiya, Y. Ando, D. Casa, T. Gog, and Y. J. Kim, Phys. Rev. B **83**, 075120 (2011).
[40] W. S. Lee, J. J. Lee, E. A. Nowadnick, S. Gerber, W. Tabis, S. W. Huang, V. N. Strocov, E. M. Motoyama, G. Yu, B. Moritz, H. Y. Huang, R. P. Wang, Y. B. Huang, W. B. Wu, C. T. Chen, D. J. Huang, M. Greven, T. Schmitt, Z. X. Shen, and T. P. Devereaux, Nat. Phys. **10**, 883 (2014).
[41] M. M. Sala, V. Bisogni, C. Aruta, G. Balestrino, H. Berger, N. B. Brookes, G. M. deLuca, D. Di Castro, M. Grioni, M. Guarise, P. G. Medaglia, F. M. Granozio, M. Minola, P. Perna, M. Radovic, M. Salluzzo, T. Schmitt, K. J. Zhou, L. Braicovich, and G. Ghiringhelli, New J. Phys. **13**, 043026 (2011).
[42] See Supplement Material at http://link.aps.org/supplemental/10.1103/PhysRevB.92.104507 for the full set of fitting curves at each q position and polarization.
[43] S. M. Hayden, G. Aeppli, T. G. Perring, H. A. Mook, and F. Doğan, Phys. Rev. B **54**, R6905 (1996).
[44] V. Bisogni, L. Simonelli, L. J. P. Ament, F. Forte, M. Moretti Sala, M. Minola, S. Huotari, J. van den Brink, G. Ghiringhelli, N. B. Brookes, and L. Braicovich, Phys. Rev. B **85**, 214527 (2012).
[45] S. Petit and M.-B. Lepetit, Europhys. Lett. **87**, 67005 (2009).
[46] D. Benjamin, I. Klich, and E. Demler, Phys. Rev. Lett. **112**, 247002 (2014).
[47] M. Magnuson, T. Schmitt, V. N. Strocov, J. Schlappa, A. S. Kalabukhov, and L.-C. Duda, Sci. Rep. **4**, 7017 (2014).
[48] Kh. Zakeri, Y. Zhang, J. Prokop, T.-H. Chuang, N. Sakr, W. X. Tang, and J. Kirschner, Phys. Rev. Lett. **104**, 137203 (2010).
[49] S. Johnston, F. Vernay, B. Moritz, Z.-X. Shen, N. Nagaosa, J. Zaanen, and T. P. Devereaux, Phys. Rev. B **82**, 064513 (2010).
[50] N. Nücker, E. Pellegrin, P. Schweiss, J. Fink, S. L. Molodtsov, C. T. Simmons, G. Kaindl, W. Frentrup, A. Erb, and G. Müller-Vogt, Phys. Rev. B **51**, 8529 (1995).

[51] J. Fink, N. Nücker, E. Pellegrin, H. Romberg, M. Alexander, and M. Knupfer, J. Electron. Spec. Rel. Phenom. **66**, 395 (1994).

[52] M. Merz, N. Nücker, P. Schweiss, S. Schuppler, C. T. Chen, V. Chakarian, J. Freeland, Y. U. Idzerda, M. Kläser, G. Müller-Vogt and Th. Wolf, Phys. Rev. Lett. **80**, 5192 (1998).

[53] M. Salluzzo, G. Ghiringhelli, J. C. Cezar, N. B. Brookes, G. M. De Luca, F. Fracassi, and R. Vaglio, Phys. Rev. Lett. **100**, 056810 (2008).

[54] P. Kuiper, G. Kruizinga, J. Ghijsen, M. Grioni, P. J. W. Weijs, F. M. F. de Groot, G. A. Sawatzky, H. Verweij, L. F. Feiner, and H. Petersen, Phys. Rev. B **38**, 6483 (1988).